JOURNAL OF PETROLOGY | VOLUME 42 | NUMBER 12 | PAGES 2197–2214 | 2001

Secular Geochemistry of Central Puerto Rican Island Arc Lavas: Constraints on Mesozoic Tectonism in the Eastern Greater Antilles

WAYNE T. JOLLY[1]*, EDWARD G. LIDIAK[2], ALAN P. DICKIN[3] AND TSAI-WAY WU[4]

[1]DEPARTMENT OF EARTH SCIENCES, BROCK UNIVERSITY, ST. CATHARINES, ONT., CANADA L2S 3A1

[2]DEPARTMENT OF GEOLOGY AND PLANETARY SCIENCES, UNIVERSITY OF PITTSBURGH, PITTSBURGH, PA 15260, USA

[3]DEPARTMENT OF GEOLOGY, McMASTER UNIVERSITY, HAMILTON, ONT., CANADA L8S 4M1

[4]DEPARTMENT OF GEOLOGY, UNIVERSITY OF WESTERN ONTARIO, LONDON, ONT., CANADA N6A 5B7

RECEIVED MAY 10, 2000; REVISED TYPESCRIPT ACCEPTED MAY 21, 2001

Island arc volcanism in the Greater Antilles persisted for >70 m.y. from Middle Cretaceous to Late Eocene time. During the initial 50 m.y., lavas in central Puerto Rico shifted from predominantly island arc tholeiites (volcanic phase I, Aptian to Early Albian, 120–105 Ma), to calc-alkaline basalts (phase II, Late Albian, 105–97 Ma), and finally to high-K, incompatible-element-enriched basalts (phases III and IV, Cenomanian–Maastrichtian, 97–70 Ma). Following an island-wide eruptive hiatus, geochemical trends were reversed in the Eocene with renewed eruption of calc-alkaline basalts (phase V, 60–45 Ma). Progressive increases in large-ion lithophile elements (LILE)/light rare earth elements (LREE), LILE/high field strength elements (HFSE), LREE/HFSE, and HFSE/heavy rare earth elements (HREE) characterize the compositional evolution of the first four volcanic phases. The shift in trace element compositions is mirrored by increasing radiogenic content of the lavas. $Pb\Delta^{8}/_{4}$ values, representing deviations of $^{208}Pb/^{204}Pb$ from the Northern Hemisphere Reference Line (NHRL), range from −20 to almost +2·0 in phases I and II, and up to +25 in phase III. Similarly, ε_{Nd} values decrease slightly from +8 to almost +6 between volcanic phases I and III. Finally, initial (i) $^{87}Sr/^{86}Sr$ values in phase I basalts have a narrow range from 0·7033 to 0·7040, near the upper limit of altered mid-ocean ridge basalt (MORB), whereas values from phases III and IV basalts have a broader range from 0·7034 to 0·7044. N-MORB-normalized incompatible element distribution patterns of Puerto Rican volcanic rocks have uniformly flat HREE segments and Y/Yb is ~1, indicating that garnet and amphibole were insignificant as residual phases and that melting occurred predominantly within relatively dry spinel lherzolite. Yb concentrations, which provide constraints on degree of melting, are consistent with a narrow range from 30 to 35% melting in volcanic phase I, but with a much broader range from 25 to 40% melting during phase III. It seems likely that such high degrees of melting were attained through a combination of flux-related melting and buoyancy-driven pressure-release fusion. Nb abundances, which reflect degree of incompatible element enrichment compared with fertile MORB mantle (FMM), are low in volcanic phase I, consistent with ~2% low-degree pressure release melting of source material in the back-arc region before entry into the arc melting zone. Subsequent lavas from phases II and III have N-MORB-like or higher Nb abundances, indicating that (1) back-arc processes peaked in intensity during the first 10–20 m.y. and later declined in significance, and/or (2) the degree of incompatible element enrichment gradually increased as a result of subduction of a thickening accumulation of pelagic sediment. Isotope mixing models indicate that the proportion of authigenic pelagic sediment incorporated into Puerto Rican basalts increased from negligible levels in phase I to as high as 2% in phases III and IV. Although the absolute magnitude of the sediment component increased progressively, a narrow range of Th/La in mafic end-members indicates that the terrigenous contribution remained uniform throughout volcanism, consistent with the insular setting of the eastern Greater Antilles Arc.

*Corresponding author. E-mail: wayne@craton.geol.brocku.ca

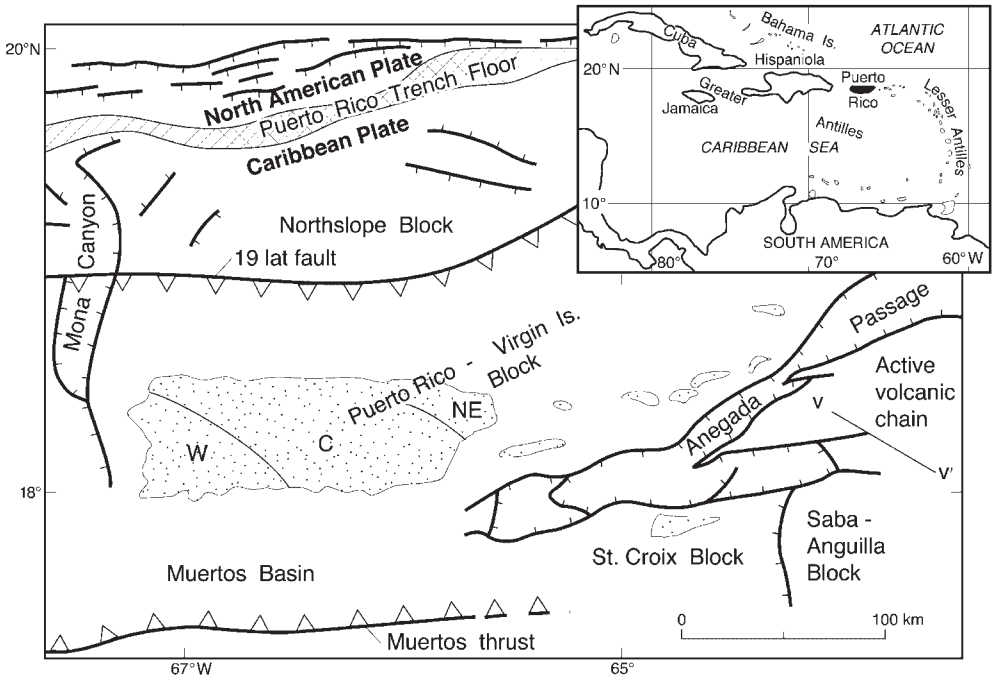

Fig. 1. Tectonic setting of the Puerto Rico–Virgin Islands and associated fault-bounded tectonic blocks (modified from Speed & Larue, 1991) of the eastern Greater Antilles Island Arc. Muertos Thrust and 19E Latitude Fault represent broad thrust zones, with teeth representing the overridden surface; scarps on faults designate downthrown sides. V–V′, westernmost active volcanic chain of the modern Lesser Antilles Island Arc.

KEY WORDS: *Cretaceous subduction; fluid flux; mantle melting; Puerto Rico; Greater Antilles; Caribbean*

INTRODUCTION

The extinct Greater Antilles Island Arc, consisting of Cuba, Hispaniola, Puerto Rico, and the Virgin Islands, represents the long-lived, intraoceanic island arc system marking the Cretaceous boundary between the modern Caribbean and North American plates (Fig. 1). The deeply dissected sequence of volcanic strata in Puerto Rico, located together with the Virgin Islands at the eastern end of the arc, ranges in age from Middle Cretaceous to Eocene and contains a complete record of all stages of arc development spanning almost 70 m.y. Island-wide geological mapping by the US Geological Survey at a scale of 1:20 000 [see summary by Jolly *et al.* (1998*b*)] has firmly established stratigraphic correlations within the sequence. As a result, the island not only represents one of the longest intraoceanic island arc sequences preserved, but also has one of the most highly constrained stratigraphic frameworks of ancient arcs in the world.

Major element geochemical data demonstrate that a profound geochemical shift, from early island arc tholeiites to late K-rich calc-alkaline assemblages, is present within the thick Puerto Rican stratigraphic succession (Glover, 1971; Mattson, 1979; Donnelly, 1989; Lebron & Perfit, 1994). Trace element studies (Jolly *et al.*, 1998*a*; Schelleckens, 1998) reveal that the geochemical progression is marked by twofold increases in abundances of the more incompatible elements, such as Th, Nb, and light rare earth elements (LREE), and by order of magnitude increases in certain incompatible element ratios, such as Th/Y and Nb/Y. The fortunate occurrence of this prominent compositional shift within such a complete and well-constrained stratigraphic framework uniquely qualifies Puerto Rico as representative of both long-term geochemical trends in maturing arc systems in general, and of the evolution of physicochemical conditions within the eastern part of the Greater Antilles subduction zone during formation of the northern boundary of the Caribbean Plate in particular.

Although investigation of an extinct island arc system produces a stratigraphic perspective not accessible in modern arcs, where recent eruptive rocks rapidly bury older strata, effects of degradation severely limit geochemical study of ancient volcanic piles. In the Greater Antilles, devitrification, zeolite-grade alteration, and other low-temperature diagenetic processes produced considerable scatter in distribution of the large-ion lithophile elements (LILE; Rb, Ba, K, Sr) as a result of pervasive mobilization of these soluble components. To

avoid secondary effects, the focus of this investigation is concentrated on the less soluble rare earth elements (REE) and high field strength elements (HFSE), and the highly incompatible but relatively insoluble element Th. This group of components, when considered jointly with Pb, Nd, and Sr isotope data, provides insight into crustal and mantle processes involved in island arc petrogenesis. The principal objectives of this paper include the following: (1) geochemical classification of the Puerto Rican volcanic suite and determination of the role of subvolcanic fractional crystallization (fc); (2) evaluation of the modal composition and melting patterns in the peridotite source (mantle wedge component, MC), primarily using HFSE and heavy REE (HREE) abundances, with a view toward providing constraints on Late Mesozoic subduction parameters in the eastern Greater Antilles subduction zone and the associated back-arc region; (3) estimation of the composition and relative abundance of the subduction-related component (SC), from variations in isotope compositions and Th–REE abundances, with the purpose of identification of subducted pelagic sediments, and estimation of the relative proportions of terrigenous material subducted by the Greater Antilles Arc during Late Cretaceous time.

GEOLOGICAL SETTING

The island of Puerto Rico, on the eastern flank of the Greater Antilles, is located south of the broad, structurally diffuse Puerto Rico Trench, which forms the boundary between the North American and Caribbean plates (Fig. 1). The modern island is aligned with the west-trending Trench and Muertos Trough, which represent the north and south borders of the fault-bounded Puerto Rico–Virgin Islands block and associated Northslope block (Speed & Larue, 1991), respectively. West of Puerto Rico lie the Mona Passage and Hispaniola. To the east across the Anegada Passage are the Virgin Islands and the westernmost active volcanic chain of the modern Lesser Antilles Arc (denoted V–V′ in Fig. 1).

A deformed southward-dipping Tertiary subduction zone is preserved in the upper mantle beneath modern eastern Puerto Rico (Sykes *et al.*, 1982). However, the polarity of subduction during Cretaceous time has not been established in any of the islands of the Greater Antilles Arc system. Investigators agree that subduction was preceded by generation of the proto-Atlantic Ocean, the southwestern (proto-Caribbean) arm of which bridged the developing gap between North and South America (Burke, 1988; Donnelly, 1989; Pindell & Barrett, 1990). The proto-Caribbean arm became extinct at ~125 Ma, initiating convergence between the North American and Pacific (Farallon) plates. Structural and stratigraphic evidence of major tectonic discontinuities is absent in Puerto Rico until ~85 Ma (mid-Santonian; Jolly *et al.*, 1998*b*). At that time left-lateral strike-slip faulting shortened the arc and juxtaposed the fault-bounded central and northeastern volcanic provinces (denoted C and NE, respectively, in Fig. 1). A second period of tectonism uplifted and exposed the entire island to erosion during the Paleocene (Donnelly *et al.*, 1990; Pindell & Barrett, 1990). Arc volcanism finally terminated during the Late Eocene following collision of the arc with the Bahama Islands. In subsequent Oligocene time, eastern Puerto Rico was rotated 30°E counterclockwise to its present position (Reid *et al.*, 1991).

Development of the Puerto Rican arc platform

Arc-related crust in eastern Puerto Rico is unusually thick, reaching a maximum in the NE of ~30 km (Boynton *et al.*, 1979). Measured stratigraphic thicknesses reach only ~14 km in the central part of the island (Jolly *et al.*, 1998*b*). Donnelly *et al.* (1990) suggested that the balance represents underplating by arc-related intrusive bodies (Lidiak & Jolly, 1996*a*). The volcanic core of the island consists of three volcanic provinces (Figs 1 and 2), separated by major left-lateral strike-slip fault zones of mid-Santonian age. Cretaceous volcanic centers occur in four subparallel east-trending belts (Fig. 2), analogous to volcanic fronts of modern island arcs (see, e.g. Carr *et al.*, 1990), each of which formed along the northern flank of precursors. The oldest deposits (volcanic phase I, Aptian to Early Albian age, ~120–105 Ma) contain basalts and related volcanic rocks resembling modern low-K island arc tholeiites (Fig. 2a). Slightly younger strata (phase II, Late Albian to Cenomanian, 105–90 Ma) contain predominantly calc-alkaline basalts and felsic derivatives with $CaO/(Na_2O + K_2O) \sim 1$ (Fig. 2b). Subsequent units (phases III and IV, Cenomanian to mid-Maastrichtian, 90–70 Ma) contain high-K basalts (Fig. 2c and d). Geochemical trends were reversed during the Early Tertiary (phase V, Paleocene to Eocene age) when felsic calc-alkaline flows and pyroclastic rocks, not considered in this investigation, dominated volcanism. Emphasis in this paper is on the three initial volcanic phases erupted before strike-slip faulting associated with juxtapositioning of the central and northeastern volcanic provinces. However, the petrographic character of phase IV volcanic rocks is considered and their geochemical fields, which overlap those of phase III, are included in variation diagrams for reference.

Petrography of the Puerto Rican volcanic suite

Lavas in central Puerto Rico are predominantly devitrified basalts with abundant, commonly euhedral

phenocrysts of labradorite, ferroaugite, and chloritized pseudomorphs of olivine (Jolly *et al.*, 1998*a*), all characteristic products of low-total pressure (low-P_t) subvolcanic gabbroic fractionation. Hornblende is absent from all eruptive rocks in volcanic phases I–IV, but is present in a few stocks and sills of Late Cretaceous age (Pease, 1968; Glover, 1971). Accessory minerals include apatite and subhedral magnetite grains. Perchas basalts from phase III (Fig. 2c), contain sparse orthopyroxene invariably degraded to chlorite. Even though relict mineralogy and degree of alteration are monotonous throughout the sequence, textures and phenocryst proportions are distinctive such that individual units are readily recognizable. Post-depositional diagenesis and zeolite and prehnite–pumpellyite metamorphism has recrystallized or overprinted original groundmasses of Puerto Rican volcanic rocks (Cho, 1991), but relict textures and phenocrysts of augite and partly albitized plagioclase are preserved in most specimens. Stratigraphic reconstructions and secondary mineral compositions indicate that metamorphism occurred at shallow levels, normally <1·5–3 km. Cho (1991) suggested that widespread subvolcanic plutonic activity associated with volcanism elevated regional geothermal gradients.

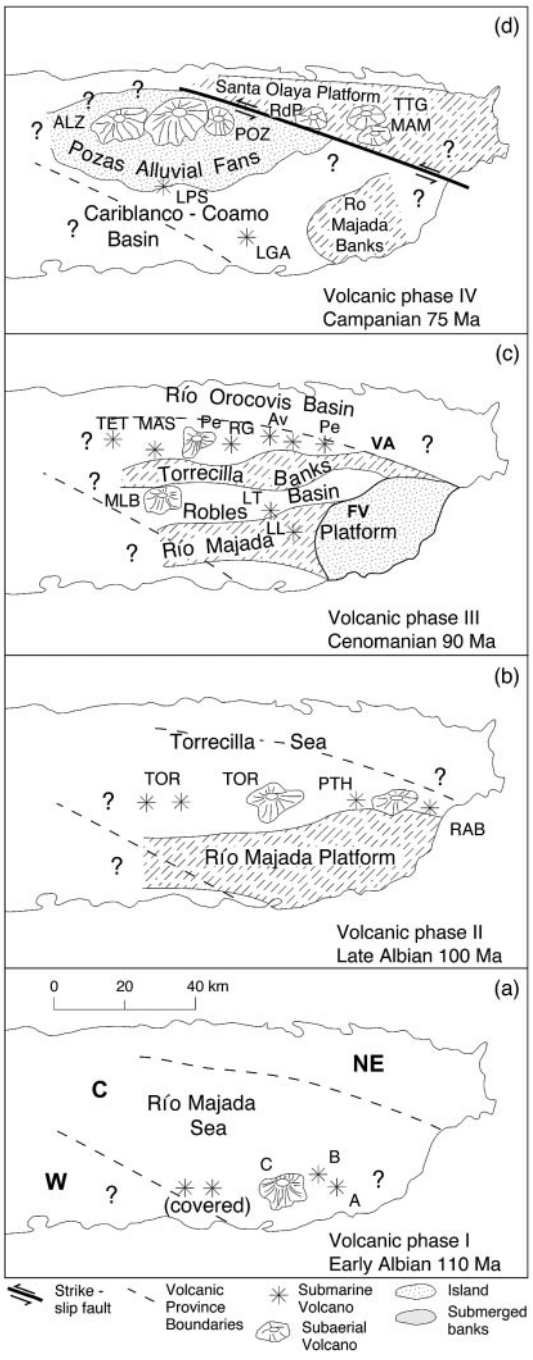

Fig. 2. Paleogeographic evolution of the eastern Puerto Rican arc platform. (a) Early Albian, 110 Ma (volcanic phase I), marine (Formations A and B) and subaerial (Formation C) strato-volcanic accumulations. (b) Late Albian, 100 Ma (volcanic phase II); subaerial to partly subaerial Torrecilla and Pitahaya volcano-stratigraphic belt; TOR, Torrecilla Breccia; PTH, Pitahaya Fm; RAB, Río Abajo Fm. (c) Cenomanian, 90 Ma (volcanic phase III), marine to subaerial Río Orocovis volcano-stratigraphic belt; units from the main volcanic axis (VA) include: TET, Tetuán Fm; MAS, Mameyes Lava; MLB, Malo Breccia–Cotorra Tuff; Pe, Perchas Lava; RG, Río Grande Pluton (subvolcanic equivalent of Perchas basalt); Av, Avispa Lava (late-stage, post Perchas lavas). Flank volcanic (FV) units include: LL, Lapa Lava; LT, Las Tetas Lava. (d) Campanian, 75–80 Ma (volcanic phase IV), Pozas and Alonzo Formations, pyroclastic and epiclastic alluvial fans; left-lateral movement on the Cerro Mula Fault juxtaposed the northeastern volcanic province. ALZ, Alonzo Fm; POZ, Pozas Fm; RdP, Río de la Plata Sandstone; TTG, Tortugas Andesite; MAM, Mamey Lava; LPS, Los Panes Stock; LGA, La Guaba Lava of Cariblanco Formation.

ANALYTICAL DATA AND GEOCHEMICAL PARAMETERS

Analytical techniques

Jolly *et al.* (1998*a*) summarized isotope, inductively coupled plasma mass spectrometry (ICP-MS), instrumental activation analysis (IAA), and X-ray fluorescence (XRF) trace element analytical techniques and precision limits. Nb was determined by a variety of methods, including ICP-MS and XRF techniques. Duplicate analyses by both methods in several laboratories reveal differences that are within the analytical error limit of 0·5 ppm. Rocks analyzed for Nb were ground in identical steel vessels to insure minimal contamination, and samples analyzed for isotopes were routinely leached overnight in hot concentrated HCl to minimize effects of low-temperature alteration. Duplicate analyses of unleached samples revealed no significant differences. Table 1 lists data for diagnostic elements [SiO_2 and MgO

(wt %); Th, Nb, La, Zr, Y, and Yb (ppm)] together with isotope ratios ($i^{87}Sr/^{86}Sr$, ε_{Nd}, and $Pb\Delta^{8}/_{4}$).

Geochemical parameters

Mineralogical modes of peridotite adopted for use in melting models (McKenzie & O'Nions, 1991) include: spinel lherzolite—olivine (ol) 57·8 vol. %, orthopyroxene (opx) 27·0%, clinopyroxene (cpx) 11·9%, spinel (sp) 3·3%; garnet lherzolite—ol 59·8%, opx 21·1%, cpx 7·6%, garnet (gt) 11·5%. Rates of phase disappearance during partial melting utilized in the models include cpx 30%, gt 15% and opx 45% (McKenzie & O'Nions, 1991); and Al-spinel 80% (Pearce & Parkinson, 1993). The set of incompatible element mineral–melt trace element partition coefficients (*D* values) compiled by McKenzie & O'Nions (1991), with modifications from the complementary sets of Hawkesworth *et al.* (1993*a*) and, for Th and Nb, Bédard (1999), is adopted.

Upward re-equilibration of melts with the mantle and melt retention by the residue (Johnson & Dick, 1992) are simulated in mantle melting models by combining non-modal equilibrium batch melting processes (Shaw, 1970) with corrections for trapped melt. The trapped melt is treated as a separate phase with a partition coefficient (*D* value) of 1·0, according to the method of Pearce & Parkinson (1993). This procedure increases bulk distribution coefficients for all incompatible elements, but especially for the most incompatible end-members (i.e. including Th, Nb, La, Ce, Pr, and Nd). A value of 1·0% trapped melt retention is adopted here, but retention instead of 0·5% trapped melt in source residua does not significantly alter results. Trace element inversion (INV) techniques, assuming a standardized 30% melt fraction, are utilized to estimate source compositions of selected basalts. This method involves a modification of the Shaw batch melting equation; that is $C_0 = [D_0 + f(1 - D_0)]C_L$, from equation (11) of Shaw (1970), where C_0 represents the source composition of a particular element, C_L the melt (parental basalt) composition, D_0 the bulk partition coefficient of the source, and f the estimated proportion of fusion.

DISTRIBUTION OF INCOMPATIBLE TRACE ELEMENTS

Geochemical classification of Puerto Rican arc basalts

Hawkesworth *et al.* (1993*a*, 1993*b*) subdivided island arc basalts into two groups on the basis of LREE/HREE (Fig. 3a and b). The low-LREE series (here restricted to La/Yb <5) comprises predominantly intraoceanic arcs (Tonga, South Sandwich, New Britain, Marianas, Northern Lesser Antilles, Aleutians), whereas the high-LREE series (La/Yb >5) consists of arcs developed in proximity to continental margins (Philippines, Southern Lesser Antilles, Aeolian Islands). Central Puerto Rican lavas from volcanic phase I fall entirely within the low-LREE/Yb island arc group, whereas those from phase II straddle the boundary. Lavas from phases III and IV overlap the high-LREE/Yb group, with La/Yb up to 15. Temporal trends of other incompatible trace element ratios are also enriched upward in the stratigraphic section. For example, both Th/Y and Nb/Y increase by over an order of magnitude (Fig. 4a and b), whereas Sm/Yb is doubled (Fig. 4c).

Subvolcanic fractional crystallization (fc)

Covariation of Th/La and Zr/Yb is relatively insensitive to degree of melting. Although Th/La is highly sensitive to contamination of source materials by terrigenous sediment and incompatible element-enriched ocean island basalt (McDermott & Hawkesworth, 1991), this ratio has a limited range in mafic end-members of the Puerto Rican volcanic suite, averaging ~0·120. Because fractional crystallization is the only major process affecting Th/La and Zr/Yb, their covariation provides a convenient fractional crystallization grid (Fig. 5c). The grid is based on fractionation vectors for plagioclase (plfc) and augite (cpxfc), the only major phases present in Puerto Rican lavas, together with vectors for combined fractionation of 0·75 plagioclase (pl) + 0·25 augite (cpx), 0·50 pl + 0·50 cpx, and 0·25 pl + 0·75 cpx. Mafic end-members from all volcanic phases (units A, PTH and RAB, TOR, PE, RGI) form a series of overlapping, horizontal fields subparallel to the vector 0·5 pl + 0·5 cpx. This distribution is consistent with precipitation (or accumulation) of approximately equal proportions of plagioclase and augite; simultaneous assimilation and fractional crystallization (afc) of plagioclase-rich arc-related material produces similar trends. Individual fields for more evolved units (LT, HS, Av, LL, RGII), and the overall Puerto Rican trend, shift to higher slopes, subparallel to the fractionation vector 0·75 pl + 0·25 cpx, indicating fractionation of increasing proportions of plagioclase (Fig. 5c). Felsic end-members of the Río Grande Pluton (RGII) have the most elevated Zr/Yb, representing a total of >95% crystallization. Highly evolved lavas from Formation J in phase I plot anomalously, as a result of late-stage separation of REE–Zr-rich accessories, including apatite and zircon.

MORB-normalized incompatible element distribution patterns

Mid-ocean ridge basalt (MORB)-normalized plots of incompatible trace elements reveal that Puerto Rican

Table 1: Geochemical data for SiO_2, MgO, and selected incompatible trace elements; and Pb, Nb, and Sr isotope data from central Puerto Rican volcanic rocks

Sample	SiO_2	MgO	Th	Nb	La	Zr	Y	Yb	$i^{87}Sr/^{86}Sr$	ε_{Nd}	$Pb\Delta^8/_4$
A-3*I	42·98	3·77	1·16	1·8	9·84	84	22·1	2·11	—	—	—
A-4*I	53·20	4·75	0·96	0·9	5·45	81	22·3	2·34	0·7034	7·19	—
A-5*I	53·36	5·21	0·92	0·9	0·16	72	19·8	2·12	0·7036	8·48	−16·5
A-7*I	52·80	5·11	0·50	0·7	4·77	52	17·0	1·85	—	—	—
A-8*I	55·30	4·56	0·85	1·1	7·29	71	25·1	2·90	0·7037	8·22	—
AV-148 III	55·87	8·69	2·40	3·8	13·20	114	23·0	2·53	0·7036	7·05	—
AV-159 III	57·64	2·54	3·10	4·6	18·10	142	29·5	3·16	0·7044	6·24	—
AV-54A III	57·97	1·88	2·70	3·6	17·70	120	28·6	2·99	0·7041	—	—
AV-56 III	57·57	3·05	2·90	5·7	19·80	123	28·0	3·14	0·7038	—	—
AV-74 III	56·55	2·63	2·20	2·6	14·00	86	21·1	2·29	—	—	—
AVB-43 III	58·53	1·52	7·70	4·8	34·30	128	27·2	2·90	0·7042	—	—
J-44*I	70·76	0·78	1·20	3·0	9·70	190	39·6	4·60	—	—	—
J-45*I	70·20	1·46	1·07	2·2	8·38	175	39·5	5·12	—	—	—
J-77*I	55·00	4·06	0·40	0·7	4·50	82	19·1	2·22	—	—	—
J-79*I	67·03	1·39	0·80	2·3	8·16	127	38·5	4·21	—	—	—
J-80*I	75·57	0·73	0·51	1·3	6·95	92	34·4	3·39	—	—	—
LL-11B III	54·80	2·10	4·10	4·6	16·10	97	16·1	1·72	0·7039	—	—
LL-16B III	51·50	6·48	3·30	3·6	15·30	77	14·0	1·77	0·7040	—	—
LL-37D III	55·10	4·21	3·70	1·7	17·30	72	14·0	1·78	0·7042	—	—
LL-37J III	53·51	4·21	3·30	4·0	15·40	81	17·3	1·76	0·7041	—	—
LL-38D*III	58·40	1·07	2·90	4·8	15·60	100	16·7	2·02	0·7038	6·25	18·9
LL-54A III	58·50	2·12	5·20	5·7	21·10	125	18·2	2·11	0·7038	—	—
LLL-9 III	58·60	1·87	3·30	4·6	19·70	131	28·1	3·19	0·7037	6·00	—
LT-27A III	51·60	4·47	1·20	2·0	6·66	50	15·0	1·55	0·7036	6·85	—
LT-60E III	49·00	4·74	1·30	1·7	7·48	57	17·2	1·62	0·7041	—	—
Pe-111 III	47·87	8·53	2·70	2·1	18·00	44	13·8	1·69	0·7040	—	—
Pe-115*III	47·25	8·67	1·30	3·2	10·41	53	17·2	1·83	0·7040	6·04	11·2
Pe-182 III	47·20	6·92	2·90	3·2	20·40	53	12·0	1·41	—	—	—
Pe-229 III	47·72	9·07	2·60	2·7	16·60	47	15·1	1·51	0·7040	5·09	12·7
Pe-230 III	47·71	7·52	1·70	1·7	11·80	30	9·9	1·08	0·7039	—	—
Pe-239 III	51·87	2·98	3·06	3·9	21·10	58	15·3	1·69	0·7040	—	—
RG-594*III	60·75	0·20	8·84	7·6	41·73	122	18·1	1·98	—	—	16·3
RG-595*III	49·98	8·44	2·69	2·5	19·72	48	16·2	1·42	—	—	—
RG-596*III	50·76	6·27	1·99	1·8	15·95	42	14·9	1·30	—	—	—
RG-597*III	56·03	4·04	11·66	8·3	38·09	154	16·8	2·34	—	—	—
RG-598*III	49·02	6·89	2·99	2·8	19·36	51	13·9	1·29	—	—	—
RG599A*III	48·01	9·24	2·07	1·9	16·23	42	15·0	1·32	—	—	−11·4
RG599B*III	51·53	5·99	7·08	5·3	22·23	108	15·2	1·82		9·3	
RG-601*III	58·89	2·39	11·53	8·2	26·88	159	15·8	2·34	—	—	—
RG-602*III	46·87	9·08	2·01	1·8	15·74	41	15·3	1·29	—	—	6·3
RG-604*III	59·07	1·07	11·44	8·2	38·58	139	17·4	2·06	—	—	—
PTH-22*II	53·90	4·87	1·77	1·0	11·96	50	18·1	1·75	0·7037	6·52	−12·1
PTH-23 II	40·79	9·46	0·82	1·3	5·58	31	12·1	1·08	—	—	—
PTH-50 II	48·36	9·84	0·84	1·0	6·65	32	10·8	1·40	0·7039	—	−8·5
PTH-51 II	49·81	5·51	0·77	0·9	7·46	44	16·6	1·64	—	—	—
RAB-53*II	52·70	5·26	1·13	1·8	7·58	84	19·1	2·03	—	—	—
RAB-54*II	60·70	2·65	1·16	2·2	7·81	83	19·9	2·42	—	—	—
TOR-42*II	48·06	8·07	1·33	2·3	10·46	58	17·1	1·82	—	—	—
TOR-46 II	51·06	6·30	1·07	1·2	9·26	39	16·8	1·67	0·7042	8·06	—
TOR-48*II	50·70	6·40	1·05	1·4	9·20	38	16·7	1·60	—	—	—
TOR-52*II	50·23	3·84	0·80	0·9	6·28	38	16·2	1·51	—	—	—
CAJ-103B*	61·45	7·70	0·18	1·5	2·62	65	22·0	2·33	0·7043	8·92	−7·81

I, II, and III refer to Puerto Rican volcanic phases from Fig. 2. Additional data and sample locations have been given by Jolly *et al.* (1998*a*). Key to trace element analyses: *XRF and ICP-MS methods, Memorial University of Newfoundland (MUN); others by XRF and INAA methods, University of Western Ontario (UWO); trace elements in ppm, oxides in wt %. $i^{87}Sr/^{86}Sr$, initial Sr isotope ratios; ε_{Nd}, initial Nd isotope ratios with respect to the chondrite universal reference (CHUR); $Pb\Delta^8/_4$, deviation of $^{208}Pb/^{204}Pb$ from the Northern Hemisphere Reference Line (NHRL) with respect to $^{206}Pb/^{204}Pb$.

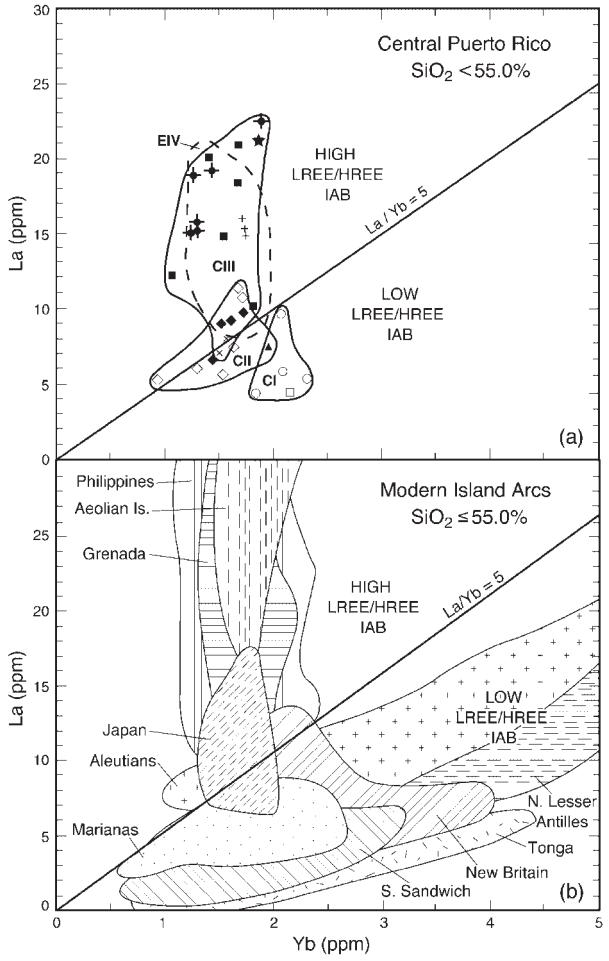

Fig. 3. La–Yb abundances in central Puerto Rican volcanic rocks. (a) Fields (CI, CII, and CIII) enclose central Puerto Rican volcanic phases I, II, and III, respectively; symbols as in Fig. 6. Dashed field of phase IV (EIV), which occurs in both the central and northeastern volcanic provinces, is included for comparison. (b) La–Yb abundances in modern island arcs. Sources of arc data are as follows: Aeolian Islands, Ellam *et al.* (1988); Central Aleutians, Romick *et al.* (1990); Grenada, Thirlwall & Graham (1984); Japan, Tatsumi *et al.* (1988); Northern Lesser Antilles, Davidson (1986), White & Dupre (1986); Marianas, Woodhead (1988); New Britain, Woodhead & Johnson (1993), Woodhead *et al.* (1998); Philippines, Defant *et al.* (1990), McDermott *et al.* (1993); South Sandwich, Cohen & O'Nions (1982); Tonga, Ewart & Hawkesworth (1987).

volcanic rocks, like Cretaceous lavas and granitoids from other islands of the Greater Antilles (Donnelly, 1989; Lebron & Perfit, 1994; Lidiak & Jolly, 1996*a*), are uniformly over-enriched in LILE with respect to LREE, moderately enriched in LREE and Th, and strongly depleted in HFSE, all fundamental features of island arc associations. Compared with other members of the Puerto Rican volcanic assemblage, phase I basalts are the least enriched in incompatible elements, and have the lowest LILE/HFSE and HFSE/HREE (Fig. 6a). In addition, they have the lowest LREE/HFSE and LREE/HREE. Values of all these ratios increase in succeeding volcanic phases, reaching maximum levels in high-K basalts from phase III (Perchas basalt, Fig. 2c). A series of flows from the upper part of volcanic phase I (Formations B and C) are relatively depleted in Th, Nb, and LREE and, as a result, have anomalous flattened to slightly depleted N-MORB-normalized REE patterns (Jolly *et al.*, 1998*b*). Trace element and isotope melting models presented elsewhere indicate that the patterns are consistent with recycling of source material in the mantle wedge (Jolly *et al.*, 2001).

Wedge- and subduction-related components

Although aqueous fluids are several orders of magnitude less efficient than magmas as transporters of incompatible elements (Hawkesworth *et al.*, 1993*a*, 1993*b*), they are abundant in arc environments as a result of dehydration reactions in the downgoing oceanic crust (Pearce, 1983; Arculus, 1994; Stolper & Newman, 1994; Pearce & Peate, 1995; Tatsumi and Eggins, 1995; Tatsumi & Kogiso, 1997), and are likely sources of wedge contamination (Keppler, 1996; Ayers, 1998). Ionic potential [the ratio of the ionic charge ($\mathcal{Z}$) and the ionic radius (r) of the element in its normal oxidation state] provides a measure of the mobility of an element in aqueous fluids (Fig. 6b). Elements with ionic potentials <2 are mobile because of formation of soluble chloride complexes (Keppler, 1996). Conversely, elements with $\mathcal{Z}/r$ between three and seven do not complex with Cl and are relatively immobile in aqueous fluids (Bailey & Ragnarsdottir, 1994; Brenan *et al.*, 1995; Lidiak & Jolly, 1996*b*).

Plots of ionic potentials (Fig. 6b) and N-MORB-normalized island arc basalt patterns (Fig. 6c) have similar features, which are utilized to apportion incompatible elements into wedge and subduction-related components. The MC is delimited by the line formed by the highly insoluble elements Nb–Zr–Y–HREE. Because these elements are added to the mantle by certain enrichment processes, such as silicate magmatism, this procedure yields the maximum MC. The SC, contributed primarily by fluids generated in the slab, or by leaching within the wedge (Hawkesworth *et al.*, 1993*a*, 1993*b*), is itself subdivided into two end-members: (1) positive spikes above the line Th–La–Ce–Nd–Sm–Eu (representing over-enrichment in LILE with respect to REE) comprise the LILE-bearing end-member of the SC. This end-member is unsuited to geochemical evaluation in ancient volcanic rocks because of elemental redistribution during low-temperature alteration, and is not considered further. (2) The area between lines Nb–Zr–Y–HREE and Th–La–Ce–Nd–Sm–Eu (Fig. 6c) represents the minimum Th–REE-bearing end-member, probably contributed by an H_2O-saturated, low-degree silicate melt derived primarily from subducted sediment (Nicholls *et al.*, 1994). The

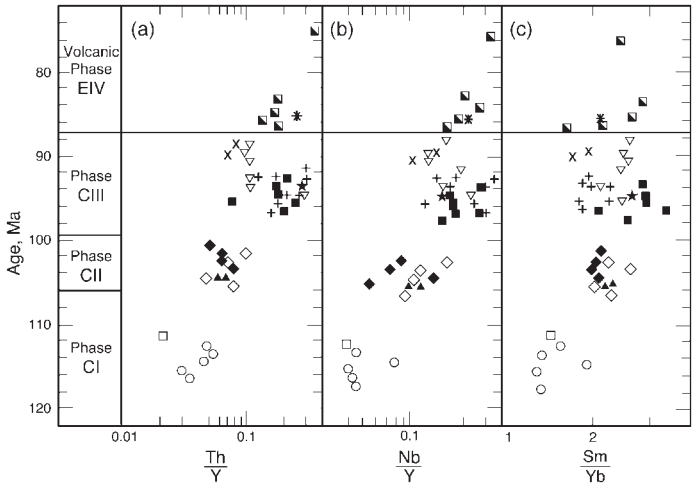

Fig. 4. Geochemical stratigraphy in central Puerto Rico. Selected ratios of analyzed samples are plotted according to approximate age, estimated from position in the stratigraphic section (Jolly *et al.*, 1998*a*). Volcanic phases from Fig. 2 are listed at left; a tectonic discontinuity between phases CIII and EIV is denoted by a horizontal line. Symbols as in Fig. 6. (a) Th/Y; (b) Nb/Y; (c) Sm/Yb.

Th–REE-rich end-member forms the basis for examination of the SC in this investigation.

THE MANTLE WEDGE COMPONENT (MC)

Composition of Atlantic and Caribbean Mesozoic MORB

Altered basalts and amphibolites associated with partly serpentinized peridotite in western Puerto Rico represent pre-arc Jurassic oceanic crust (Jolly *et al.*, 1998*b*). These basalts have MORB-like ε_{Nd} values (average $\sim$9·0) and elevated initial $(i)^{87}Sr/^{86}Sr$ (average 0·7038), overlapping the field of Cretaceous Atlantic MORB (averaging 0·7040; Jahn *et al.*, 1980), and the field of altered basalts from the Caribbean Cretaceous Basalt Province (88 Ma; Donnelly, 1994; Jolly *et al.*, 1998*a*). Pre-arc basalts have depleted normalized incompatible element patterns. They also have low La/Sm and La/Nb, averaging about 0·90 and 1·50, similar to Cretaceous Atlantic MORB (Jahn *et al.*, 1980) and N-MORB (0·95 and 1·07; Sun & McDonough, 1989). Available data, therefore, indicate that both plates associated with Greater Antilles subduction had fertile MORB mantle (FMM)-type upper-mantle compositions.

Melting regime

HFSE (Nb, Ta, Zr, Hf, Ti) have high ionic potentials ($\mathcal{Z}/r$), rendering these elements insoluble in aqueous fluids (Pearce, 1983). Hence, abundances are virtually independent of aqueous flux from the descending slab. Island arc magmas typically carry low concentrations of HFSE compared with REE and LILE, producing characteristic negative normalized Nb and Zr anomalies (Fig. 6). Theoretical (Arculus & Powell, 1986), experimental (Ryerson & Watson, 1987; Ayers, 1998) and observational (Ewart & Hawkesworth, 1987; McCullouch & Gamble, 1991; Pearce & Peate, 1995) data cast doubt on the stability of titanates in modern arc environments, and indicate instead that HFSE depletions reflect low abundances of these elements in the wedge. HFSE distribution in the Puerto Rican suite is summarized in Fig. 7a, where Nb/Zr is compared with absolute Nb concentrations. Intermediate and felsic samples with SiO_2 >55% are omitted to minimize effects of fractional crystallization of plagioclase (plfc) and augite (cpxfc), both of which have $D_{Nb} \approx D_{Zr}$. Like modern arc lavas, Puerto Rican basalts overlap the MORB field, consistent with MORB-like melting ($D_{Nb} < D_{Zr}$) rather than with retention of residual phases ($D_{Nb} > D_{Zr}$). Also as in many modern arc lavas (Ryerson & Watson, 1987; McCullouch & Gamble, 1991), mafic end-members are depleted in Nb and Zr compared with N-MORB (Fig. 7a).

Puerto Rican lavas have uniformly flat N-MORB-normalized HREE segments (Ho to Lu), denoted by $(Y/Yb)_N \approx 1{\cdot}0$ (Fig. 6a). Consequently, covariation of Nb/Zr–Y/Yb is aligned along spinel peridotite rather than more fractionated garnet peridotite melting vectors. The scarcity of convex-downward N-MORB-normalized REE patterns (Fig. 6a) also excludes amphibole as a significant residual phase in the mantle source. Thus, normalized incompatible element patterns are consistent with melting in a relatively dry spinel lherzolite source, an interpretation consistent with the absence of hornblende as a phenocryst phase in even the most felsic end-members.

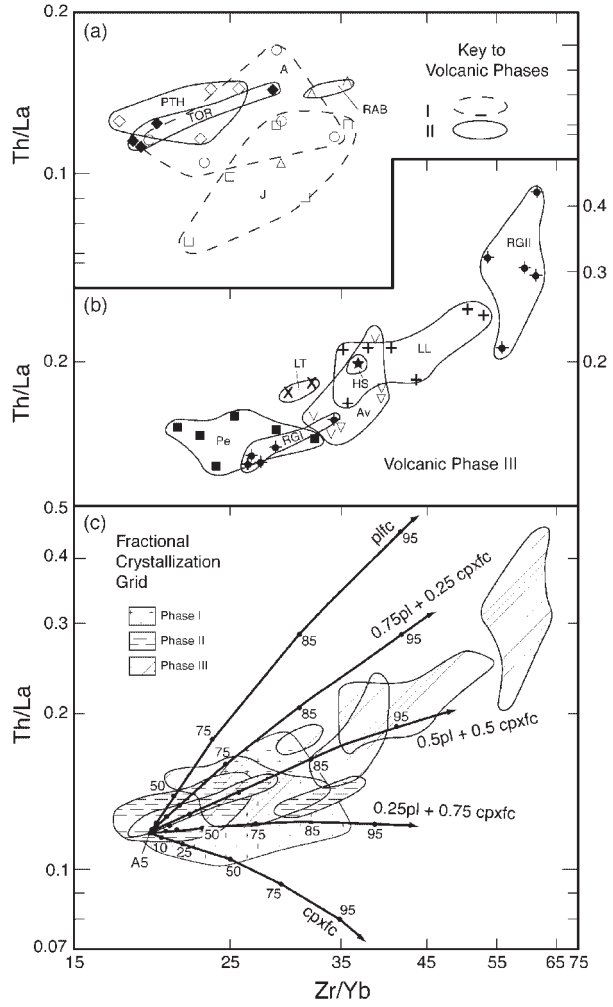

Fig. 5. Th/La vs Zr/Yb in central Puerto Rican lavas. (a) Volcanic phases I and II. (b) Volcanic phase III. (c) Fields of Puerto Rican units plotted on a fractional crystallization grid, constructed from calculated fractionation vectors for pure plagioclase (plfc) and augite (cpxfc) together with vectors for mixed assemblages (0·75pl + 0·25cpxfc; 0·5pl + 0·5cpxfc; 0·25pl + 0·75cpxfc); tick marks indicate per cent crystallization.

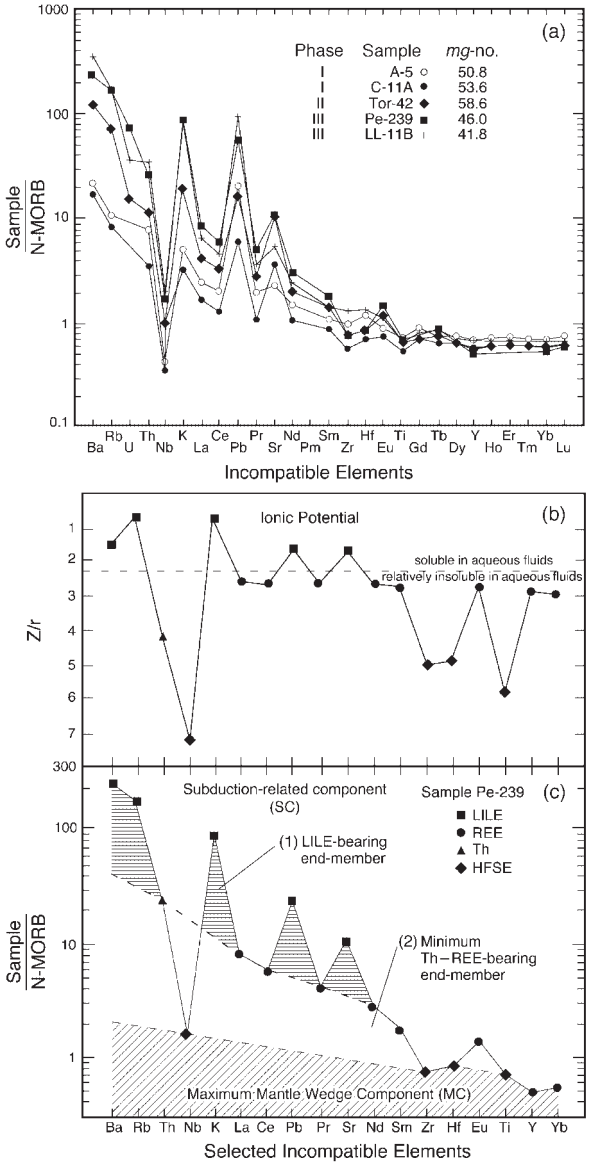

Fig. 6. (a) N-MORB-normalized elemental distribution diagrams of representative central Puerto Rican volcanic rocks (N-MORB values of Sun & McDonough, 1989). *mg*-number = Mg/(Mg + Fe). (b) Ionic potentials (Z/r) of some selected incompatible elements (modified from Pearce, 1983), arranged from left to right in the order of increasing incompatibility in N-MORB. (c) N-MORB-normalized Perchas basalt Pe-239 (the most highly incompatible element-enriched sample from volcanic phase III), illustrating the maximum MC and two end-members of the SC, including: (1) the LILE-bearing aqueous fluid end-member, and (2) the minimum Th–REE-bearing subduction-related end-member. (See text for discussion.)

Constraints on melting parameters are estimated from Nb–Y covariations according to the approach of Pearce & Parkinson (1993). Use of this elemental pair is appropriate not only because Yb concentrations reflect degree of melting, but also because absolute Nb abundances are indicative of the relative degree of incompatible element source enrichment (Fig. 8). In this procedure, MgO–Y covariations are utilized to correct MgO content of rocks to 9% to account for olivine fractionation during melt elevation from mantle depths (Fig. 8a). Although it is unlikely that all parental arc magmas had identical MgO concentrations, the technique provides a convenient comparison between individual samples within a particular arc, as well as between various arc systems generated in spinel peridotite sources. The melting grid on Nb–Yb plots is established employing melting curves for both FMM and the residue of a 5% melt of FMM. The FMM melting curve further subdivides the field of peridotite into enriched and depleted portions.

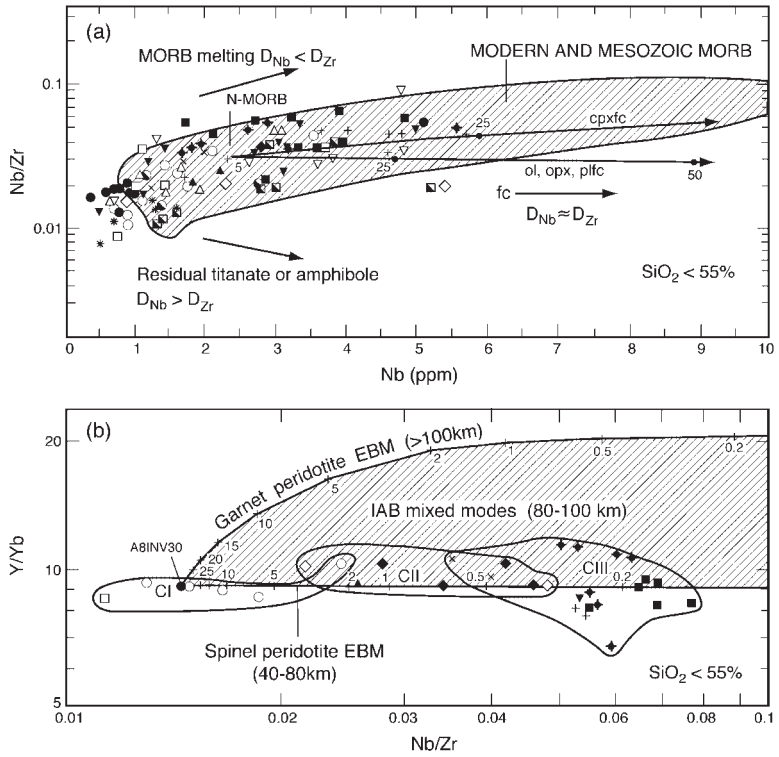

Fig. 7. (a) Nb/Zr vs absolute Nb abundances plotted according to the method of McCullouch & Gamble (1991). The field of modern MORB is from Le Roux *et al.* (1983) and Floyd (1986). Symbols as in Fig. 6. D_{Nb} and D_{Zr} represent bulk partition coefficients for Nb and Zr, respectively. Calculated fractionation vectors for sample A8, with ticks representing the per cent crystallization, for plagioclase (plfc) and augite (cpxfc) are included. (b) Y/Yb vs Nb/Zr in central Puerto Rico; volcanic phase fields as in Fig. 3a. Partial melting vectors are included for non-modal equilibrium batch melting (EBM) of the inversion source (denoted A8INV30) of sample A8 for 30% melting in spinel and garnet peridotite; IAB, island arc basalt. Limits of peridotite facies are from McKenzie & O'Nions (1991).

Results for central Puerto Rico are illustrated in Fig. 8b, where corrected fields of basalts from volcanic phases I, II, and III are denoted CI9, CII9, and CIII9, respectively. Yb concentrations average ~1·0 throughout the suite, but the range increases significantly from 30 to 35% in phase I to between 25 and 40% in phase III. Such high degrees of melting appear to conflict with petrographic and geochemical evidence that Puerto Rican melts were generated in relatively dry source materials. Therefore, it is likely that buoyancy-driven decompression melting supplemented flux-related melting within the wedge, as suggested by Davies & Stevenson (1992), Pearce & Parkinson (1993), and Parkinson & Arculus (1999). Compared with fields of modern arc suites (from Pearce & Parkinson, 1993) that have flat N-MORB-normalized HREE segments (consistent with fusion in spinel peridotite), early Puerto Rican units from volcanic phase I overlap Tonga, but are less depleted than South Sandwich, and were derived by slightly higher degrees of melting than the Marianas (Fig. 8c). All of these suites plot below the FMM melting vector, indicating that the source was depleted in the more incompatible components relative to FMM. Fields of later Puerto Rican basalts from phase II and, especially, phase III, in contrast, plot above the FMM melting vector, consistent with generation from relatively enriched sources, as in the northern Lesser Antilles, Vanuatu, and the Aleutians.

Back-arc processes

Abundances of HFSE and HREE in Puerto Rican basalts are slightly lower than in normal N-MORB. Yb_N (Figs 6a and 9), for example, averages 0·7 and has a narrower range from 1·1 to 0·6 in volcanic phase I, whereas Nb_N averages 0·9. Similar Nb depletions are common in many modern arc suites, and are widely attributed to an episode of low-degree, pressure-release melting in the back-arc region before entry of source material into the melting zone (Ewart & Hawkesworth, 1987; Ryerson & Watson, 1987; Plank & Langmuir, 1988; McCullouch & Gamble, 1991; Pearce & Parkinson, 1993; Arculus, 1994). In modern island arcs, a close correlation exists between the rate of subduction and the vigour of back-arc spreading (Rodkin & Rodkinvo, 1996). Arcs characterized by rapid subduction (>10 cm/yr), such as Tonga–Kermadec

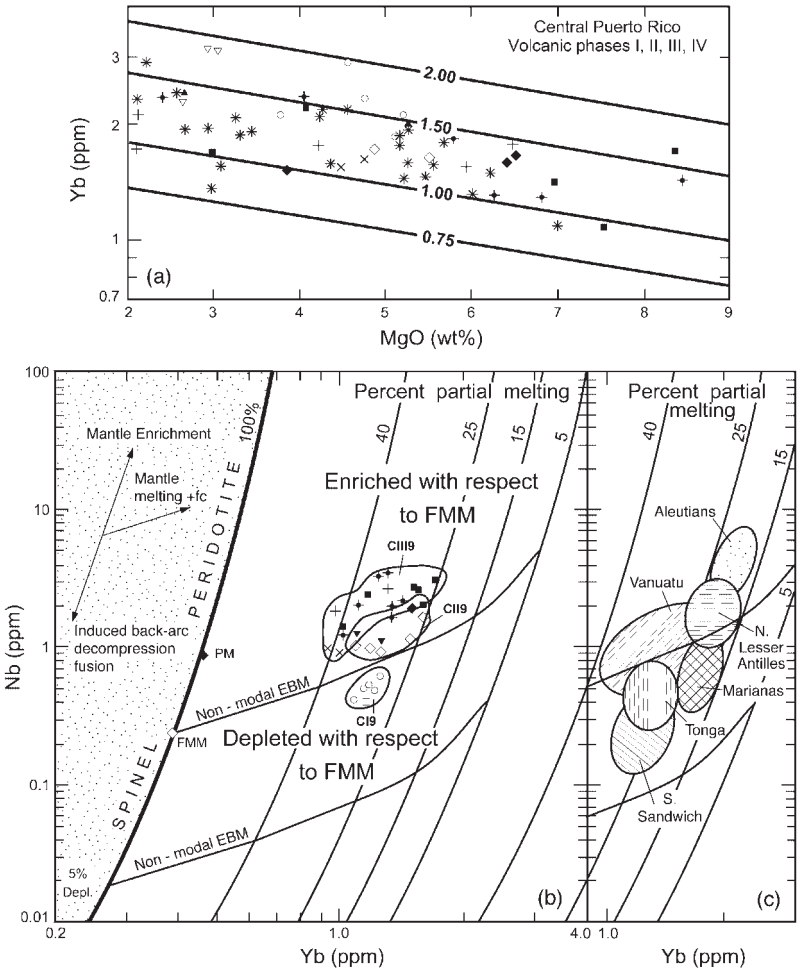

Fig. 8. (a) Covariation of MgO–Yb concentrations in central Puerto Rico. Contours illustrate the derivation and uncertainty of fractionation correction of Yb data to MgO content of 9·0 wt %; symbols as in Fig. 6. (b) Nb–Yb data from central Puerto Rico volcanic phases CI9, CII9, and CIII9, corrected to MgO content of 9·0 wt %. Spinel peridotite melting vectors (EBM) for fusion of FMM and of a residue from 5% melting of FMM are from Pearce & Parkinson (1993). PM represents the primitive mantle composition of Sun & McDonough (1989); fc, fractional crystallization; symbols as in Fig. 6. (c) Covariation of corrected Nb–Yb in selected modern island arc suites with flat N-MORB-normalized HREE patterns (fields from Pearce & Parkinson, 1993).

(Ewart & Hawkesworth (1987) and New Britain (Woodhead & Johnson, 1993; Woodhead *et al.*, 1998), have highly depleted Nb_N (as low as 0·05). Pearce & Parkinson (1993) maintained that the lowest Nb abundances in arcs reflect logarithmic rather than linear depletions, indicating loss of melt in the back arc rather than recycling of depleted mantle source material within the wedge. At the other extreme, arcs with low subduction rates, such as the northern Lesser Antilles (3·7 cm/yr, Jarrard, 1986), have minimal back-arc volcanism and little or no HFSE depletion (Thirlwall *et al.*, 1994).

Analysis of relative motions between the Pacific and Atlantic plates (Fig. 9a) during Late Mesozoic time (Pindell *et al.*, 1988; Donnelly, 1989) reveals that the convergence rate in the Greater Antilles averaged 6 cm/yr. This moderate rate is consistent with the small degree of Nb depletion observed in Puerto Rican volcanic phase I, relative to the FMM melting curve, and is indicative of limited back-arc processing of source material. Phases III and IV have higher Nb concentrations, indicating that (1) back-arc processes peaked in intensity during the initial 10–20 m.y. and thereafter declined, and/or (2) the degree of incompatible element enrichment gradually increased (Fig. 8b) as a result of subduction of a thickening accumulation of pelagic sediment.

Constraints on subduction parameters

Paleogeographic reconstructions of the Puerto Rican arc platform reveal that during volcanic phases III and IV, volcanic accumulations developed on the southern flank

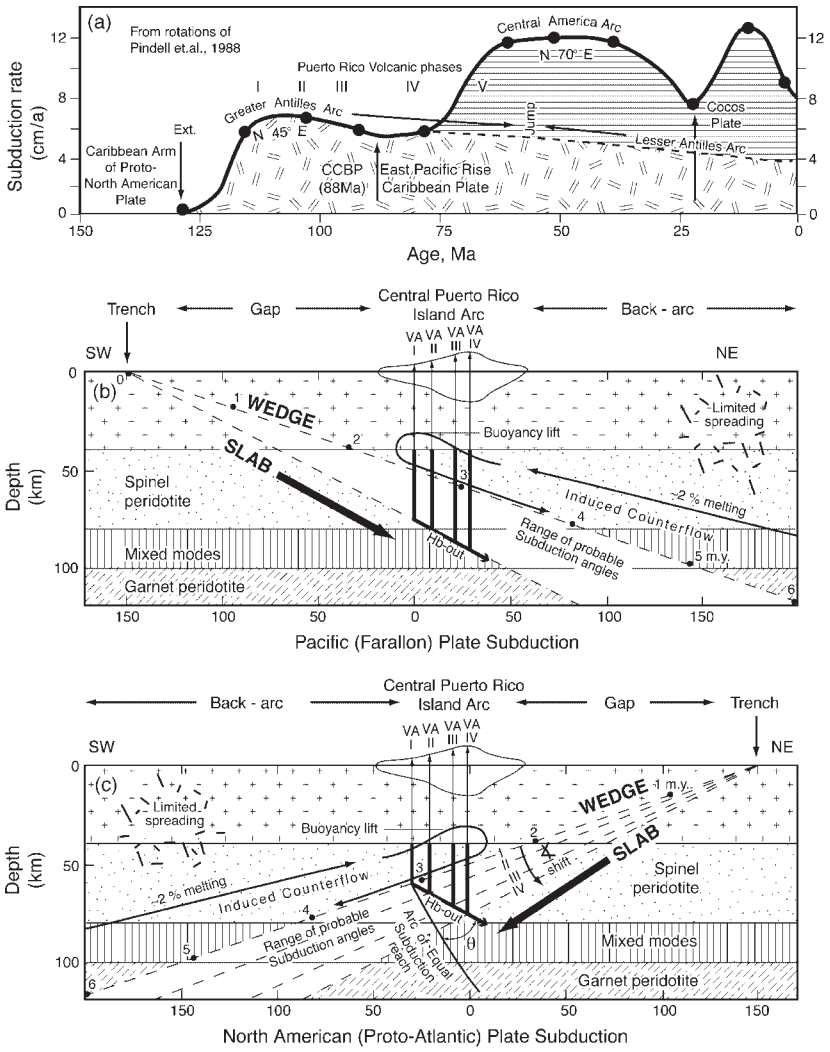

Fig. 9. (a) Convergence between North American and Pacific plates from rotations of Pindell *et al.* (1988). Arrows indicate activity along oceanic ridges; CCBP, Caribbean Cretaceous Basalt Province (Donnelly, 1994); I–V, Puerto Rican volcanic phases. Subduction rate in the early Lesser Antilles has not been established and is assumed to decay progressively (dashed line) to the modern rate of 3·7 cm/yr (Jarrard, 1986). (b) and (c) schematic scale models (km) of central Puerto Rican Cretaceous subduction in a McKenzie & O'Nions (1991) mantle model. Minimum gap between the trench and arc platform is maintained at 150 km. Range of probable subduction angles in central Puerto Rico, consistent with melting in relatively pure spinel peridotite, is bracketed. Schematic melting columns are designated by bold lines. Subduction of 6 cm/yr is indicated in 1 m.y. intervals along the slab-wedge boundary. Positions of principal volcanic axes (VAI–VAIV) within the volcanic platform are positioned for diagrammatic purposes vertically above the Hb-out dehydration reaction, which increases in depth with age of the subduction zone (Peacock, 1993). Induced wedge counterflow and limited associated spreading are indicated in back-arc region, and buoyancy-related counterflow (Davies & Stevenson, 1992) is also indicated. In (c) a progressive shift of the subduction angle is indicated for each volcanic phase. Angle θ is proportional to the ratio between the increase in depth of the slab (ΔP_{slab}) and increase in average depth of Hb-out equilibrium ($\Delta P_{Hb\text{-}out}$) with respect to successive volcanic phases.

of the principal volcanic axis (Fig. 2c and d), consistent with south-dipping subduction of the North American Plate. However, the polarity of subduction in the Greater Antilles is controversial (Donnelly, 1989; Pindell & Barrett, 1990; Draper *et al.*, 1996), and, in the absence of direct evidence from any of the islands, inference of subduction orientation from distribution of flank volcanism is regarded as tentative. Therefore, tectonic models involving both northeasterly-dipping subduction of the Pacific (Farallon) Plate (Fig. 9b) and southwesterly-dipping subduction of the North American Plate (Fig. 9c) are considered. In both models continuity of subduction polarity is assumed, in conformity with gradual evolution of geochemical trends and absence of regional evidence of tectonism.

Geochemical evidence that melting occurred in the spinel peridotite facies at depths between 40 and 80 km is not necessarily indicative of oblique subduction. The

Marianas arc, for example, has the highest subduction angle known (Jarrard, 1986), and yet produces basalts with consistently flat N-MORB-normalized HREE patterns (Woodhead, 1988). Subduction rate is a more reliable indicator of the dip of Benioff zones in modern intraoceanic arcs, and in general subduction angles in rapidly subducting systems are acute, whereas angles in arcs subducting at more moderate rates tend to be less steep or even oblique (Jarrard, 1986). As subduction rates in the Greater Antilles were relatively modest (Fig. 9a), schematic reconstructions employ oblique angles (Fig. 9b and c). A 150 km gap width between trench and volcanic axes (VA), typical of modern arcs, is maintained. Peridotite facies boundaries are from McKenzie & O'Nions (1991). The four sequential central Puerto Rican volcanic axes (VAI–VAIV) are positioned vertically above the dehydration of hornblende (Hb-out) in the slab. Deflections of fluid flow within the wedge are neglected, but back-arc wedge counterflow, and flux-related buoyancy (Davies & Stevenson, 1992) are included.

Secular models of thermal evolution in subduction zones reveal that geothermal gradients approach steady state in $\sim$50 m.y., and that, at constant subduction rate and shear stress, a decline in geothermal gradient coincides with increasing lithospheric thickness and depth of the Hb-out reaction (Peacock, 1993). In a Pacific subduction model (Fig. 9b), melting follows the Hb-out isotherms downward along the slab, and positions of volcanic axes retreat northward away from the trench. The melting zone migrates toward the thicker, warmer core of the overlying mantle wedge and synchronous cooling produces stable or decreasing degrees of melting. In an Atlantic subduction model (Fig. 9c), volcanic axes advance trenchward only when the subduction angle progressively steepens. The magnitude of advancement is controlled by θ, representing the ratio between increases in depth of the slab (ΔP_{slab}) and the Hb-out reaction ($\Delta P_{Hb\text{-}out}$). Hence, when $\Delta P_{slab} > \Delta P_{Hb\text{-}out}$, then $\theta > 0$ and volcanism advances northward toward the trench, whereas the melting zone is deflected trenchward. Regardless of the polarity of subduction, downward deflection of dehydration reactions along the Benioff zone is consistent with the 40 km northward migration of the volcanic axes in Puerto Rico as a result of long-term cooling of the wedge.

THE SUBDUCTION-RELATED COMPONENT (SC)

Nb/Zr as a secular indicator

In Puerto Rico Nb/Zr varies with degree of incompatible element enrichment of the source and is inversely proportional to age. Accordingly, this ratio is compared with key geochemical variables to provide insight into secular variations in magnitude and composition of the SC.

Th/La

In the absence of an ocean island basalt (OIB) component, Th/La in island arc suites is controlled by terrigenous sediment (McDermott & Hawkesworth, 1991). In Puerto Rico, mafic end-members of all volcanic phases form horizontal fields fixed along a line corresponding to a Th/La of 0·12 (Fig. 10a). This element pair also tends to remain coupled in modern island arc suites, but absolute Th/La values are variable from arc to arc, ranging in intraoceanic settings from as low as 0·03 in South Sandwich (Cohen & O'Nions, 1982) and 0·09 in the Marianas (McCullouch & Gamble, 1991) to >0·45 in the continental margin-type Aeolian Arc (Ellam *et al.*, 1988). The narrow range of Th/La in Puerto Rican lavas indicates that the bulk composition of the SC remained fixed, and that variations resulted from fluctuations in magnitude of the SC rather than a compositional shift. Low values of Th/La, in turn, confirm the intraoceanic setting of the eastern Greater Antilles Island Arc, and indicate that surrounding continental platforms [South America, Central America, and the Bahamas (Fig. 1)] made minimal contributions to the subduction zone.

$Pb\Delta^8/_4$ values

Pb isotope ratios in central Puerto Rican units follow mantle patterns, forming fields subparallel to the Northern Hemisphere Reference Line (NHRL; Hart, 1984). $Pb\Delta^8/_4$ values (Table 1), representing deviation of $^{208}Pb/^{204}Pb$ from the NHRL with respect to $^{206}Pb/^{204}Pb$ (Hart, 1984), are lowest in volcanic phases I and II, ranging from 0 to -20. Values are higher in phase III, ranging from $+10$ to almost $+20$. Additional Pb isotope data from the Río Grande Pluton extend the lower limit of $Pb\Delta^8/_4$ values in phase III to less than -5. In comparison, Pb isotope compositions in the adjacent northeastern volcanic province (denoted NE in Fig. 1c) cluster along the NHRL with values from 5 to -25 (Fig. 10b).

ε_{Nd} values

Initial Nd isotope ratios in central Puerto Rico overlap MORB values and, following patterns similar to those for Pb-isotopes, become gradually more enriched in radiogenic Nd (Fig. 10c). ε_{Nd} values of early units range from about 8·5 to 6·5, whereas phase III volcanic strata

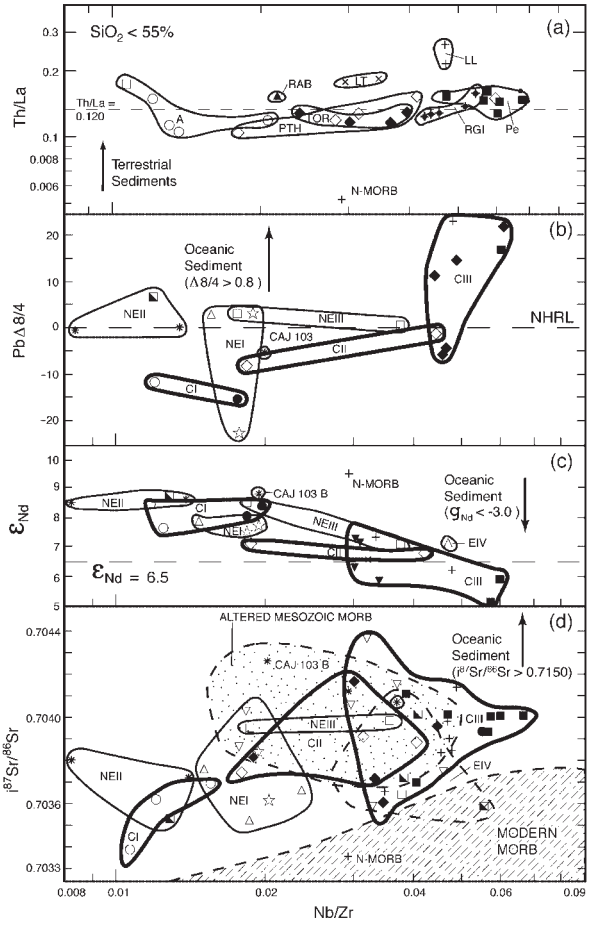

Fig. 10. Composition of the SC in central Puerto Rican lavas with SiO_2 <55%. Symbols as in Fig. 6. (a) Th/La in central Puerto Rican volcanic rocks. (b) $Pb\Delta^8/_4$ values, representing the deviation of $^{208}Pb/^{204}Pb$ from the Northern Hemisphere Reference Line (NHRL) of Hart (1984) with respect to $^{206}Pb/^{204}Pb$. (c) ε_{Nd} values. (d) Puerto Rican $^{87}Sr/^{86}Sr$ overlap the field of altered Mesozoic MORB [field includes Cretaceous Puerto Rican MORB (Jolly *et al.*, 1998*a*) and Atlantic Cretaceous MORB (Jahn *et al.*, 1980)], but exceeds modern MORB (data from Le Roux *et al.*, 1983; Floyd, 1986). Isotope data for northeastern Puerto Rico in (b), (c), and (d) are from Jolly *et al.* (1998*a*).

are distinguished by ε_{Nd} <6·5. Rocks from the northeastern volcanic province have only slight variations of ε_{Nd}, and are limited to values >6·5.

$i^{87}Sr/^{86}Sr$

Sr isotope compositions broadly approach or overlap compositions of altered Mesozoic MORB (Jolly *et al.*, 1998*a*; Fig. 10d), which is itself elevated in radiogenic content with respect to modern MORB because of seafloor alteration processes (Jahn *et al.*, 1980). Early volcanic phase I basalts have the lowest $i^{87}Sr/^{86}Sr$ (0·7033–0·7041). Basalts from phase III have higher average values (~0·7039), but the range in values (0·7035–0·7044) is larger and overlaps those of earlier units. The wider variation resembles modern highly enriched arc basalts, which also typically have a large range in $^{87}Sr/^{86}Sr$ (Hawkesworth *et al.*, 1993*b*).

Isotope mixing models

Because compositions of Late Cretaceous pelagic sediments from the Atlantic Ocean basin are unknown, meaningful trace element mixing models are not possible. Sr–Nd isotope mixing between various modern pelagic sediments and volcanic phase I basalts produce mixing curves consistent with the presence of small amounts of sediment in phases III and IV (Jolly *et al.*, 1998*a*). However, the models are poorly constrained because of the wide range in $^{87}Sr/^{86}Sr$ measured in phase III. The overlap in Sr-isotope compositions between altered MORB and arc basalts (Fig. 10d) leads naturally to the interpretation that fluids emanating from the descending oceanic crust transferred the signature of altered MORB to the mantle wedge, and subsequently to arc magmas derived from it (Hawkesworth *et al.*, 1993*b*). The broad range in $^{87}Sr/^{86}Sr$ indicates that the process was erratic and patchy, probably owing in part to compositional variation of altered MORB or to channeling of subduction-related fluid flow (as in Tonga, Turner *et al.*, 1997).

Pb–Nd and Pb–Sr isotope mixing models are more successful (Fig. 11), because addition of minute proportions of sediment radically alters Pb isotope ratios in basalts. Although the absolute composition of the mantle source is unknown, the low-$Pb\Delta^8/_4$ isotope signature of early arc basalts is similar to pre-volcanic Cretaceous MORB (Cajul basalt CAJ-103 in Figs 10b, and 11a and b), consistent with a MORB-like source (Jolly *et al.*, 1998*a*). Hence, an estimate of the proportion of sediment incorporated by more radiogenic volcanic phase III lavas, relative to initial phase I, is obtained (Fig. 11) by mixing an early sediment-poor basalt (sample A-5; Table 1) and representative modern pelagic sediments (Table 2). In $Pb\Delta^8/_4$–ε_{Nd} and $Pb\Delta^8/_4$–$i^{87}Sr/^{86}Sr$ plots, Puerto Rican data concentrate along calculated hyperbolic mixing curves involving Pacific authigenic pelagic sediment (denoted 1 in Fig. 11a and b). Phase III basalts overlap the mixing lines at the 10% level with respect to sample A-5, equivalent to incorporation of ~2% sediment with respect to FMM. As in many modern oceanic arc suites (Keller *et al.*, 1992; Woodhead *et al.*, 1998), mixing models involving $Pb\Delta^7/_4$ explain the data only if Pb isotope composition of contaminating sediments was similar to that of the basalts, with somewhat lower $^{207}Pb/^{204}Pb$ than for modern pelagic sediments.

Results of isotope models conflict with absolute Pb concentrations [6–16 ppm in volcanic phase I compared

Table 2: Modern pelagic sediment compositions utilized in mixing models (Fig. 11a and b)

	Pelagic sediment type		
	1 Atlantic detrital	2 Pacific authigenic	3 S. Atlantic biogenic
$^{208}Pb/^{204}Pb$	38·92	38·70	38·59
$^{206}Pb/^{204}Pb$	18·90	18·71	18·65
$Pb\Delta^{8}/_{4}$	46·16	45·82	41·19
Pb (ppm)	33·8	55·7	13·4
ε_{Nd}	−11·4	−4·1	−2·7
Nd (ppm)	41·5	50·0	9·4
$i^{87}Sr/^{86}Sr$	0·7161	0·7092	0·7089
Sr (ppm)	211	218	75

The table was compiled from the following sources: Hole *et al.* (1984); White *et al.* (1985); Ben-Othman *et al.* (1989); Keller *et al.* (1992); Elliot *et al.* (1997).

with a range from 3 to >65 ppm in phase III; see table 2 of Jolly *et al.* (1998*a*)], which are consistent with a total Pb contribution to the SC >50%. Similar conflicts between isotope models and trace element abundances are reported elsewhere and are commonly attributed to incorporation of additional MORB-like Pb derived from basaltic crust (Hawkesworth *et al.*, 1993*b*). Moreover, coherent isotope patterns imply that Sr, Nd, and Pb derived from sediments were coupled on entry into the fluid phase. In comparison, highly variable absolute Pb concentrations and Pb/Nd [correlation coefficient (*R*) with respect to absolute Nd = 0·35] are indicative of decoupling in the bulk fluid. These contradictory relations indicate that the LILE-bearing end-member and the sediment-rich end-member were introduced into the wedge by two successive waves of fluid flux: (1) a viscous Th–REE-rich silicate melt phase (Nicholls *et al.*, 1994) with the non-MORB-like Pb–Nd-isotope signature of pelagic sediment; (2) an LILE-rich chloride brine vapor dominated by the Sr-isotope signature of oceanic crust.

Central Puerto Rican lavas, especially samples from volcanic phases I, II, and III, are anomalously enriched in the more incompatible elements (Jolly *et al.*, 1998*a*), compared with lavas of equivalent age in the adjacent northeastern volcanic province (denoted NE in Fig. 1). As the terranes have similar Th/La, it appears unlikely that these two adjacent and simultaneous mid-oceanic arc segments subducted pelagic sediment of widely different composition. Instead, amplified enrichment in the central volcanic province probably resulted from localized lateral variation of subduction parameters, such as variation in plate convergence direction along a curving arc system, as in the Tonga–Kermadec (Ewart & Hawkesworth, 1987), Vanuatu (Peate *et al.*, 1997) and northern Marianas (Peate & Pearce, 1998) arcs. The higher degree of enrichment in central Puerto Rico is consistent with lesser obliquity of convergence compared with the northeastern province.

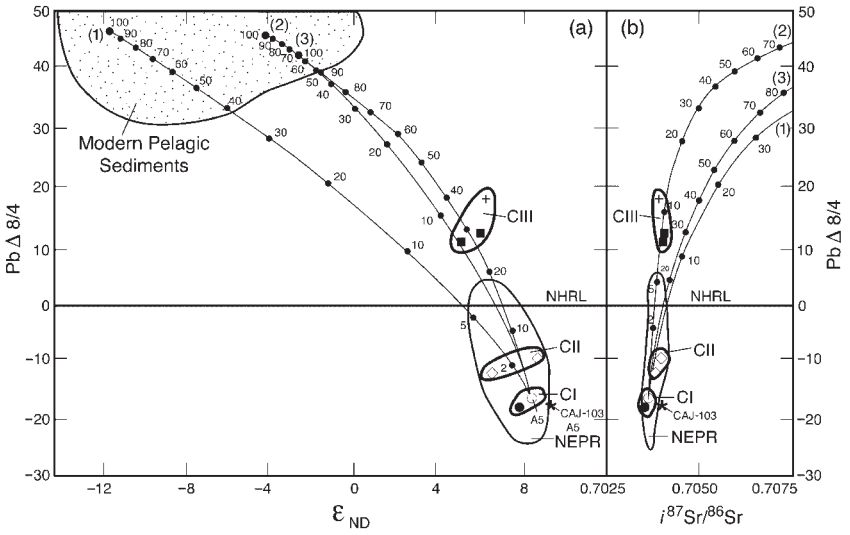

Fig. 11. $Pb\Delta^{8}/_{4}$–ε_{Nd} and $i^{87}Sr/^{86}Sr$ isotope mixing between basalt sample A-5 (Pb 6 p.p.m., Nd 10·61 p.p.m., Sr 294 p.p.m.; other data in Table 1) and representative modern pelagic sediments (see Table 2; compositions compiled from Hole *et al.*, 1984; White *et al.*, 1985; White & Dupre, 1986; Ben-Othman, 1989; Keller *et al.*, 1992; Elliot *et al.*, 1997). Fields of analyzed central Puerto Rican samples are identified as follows: CI, CII, and CIII; fields of the NE tectonic block (NEPR) and altered Puerto Rican pre-arc Cretaceous MORB basalt (sample CAJ-103) from Jolly *et al.* (1998*a*, 1998*b*).

CONCLUSIONS

The Greater Antilles Island Arc contains a complete record of subduction-related volcanism spanning >70 m.y., from Aptian time to the end of the Eocene period. Puerto Rican volcanic rocks, like their counterparts in other islands of the arc, are predominantly basaltic, but have a diverse compositional range extending from island arc tholeiites to K-rich calc-alkaline types. Regardless of relative degree of incompatible element enrichment, all members of the suite have uniformly flat N-MORB-normalized HREE patterns (Fig. 6a and c), reflected by $(Y/Yb)_N \approx 1$(Fig. 7b). The patterns are inconsistent with residual garnet or amphibole in the upper-mantle source, and indicate instead that melting occurred at relatively low P_t within the spinel lherzolite facies. The scarcity of convex-downward N-MORB-normalized REE patterns and the absence of hornblende from the phenocryst assemblage are consistent with a relatively dry source region. Paradoxically, however, covariations of Nb–Yb indicate that all magmas were generated by at least 25% melting. Presumably, therefore, flux-related melting was supplemented by buoyancy-driven decompression fusion, as in petrogenetic models of Davies & Stevenson (1992), Pearce & Parkinson (1993) and Parkinson & Arculus (1999). Convergence between the Pacific and North American plates during Late Cretaceous time produced a moderate rate of subduction in the Greater Antilles, averaging ~6 cm/yr throughout volcanic phases I–IV. This modest rate, coupled with moderate depletion of Nb in volcanic phase I, with respect to FMM, signifies limited spreading in the back-arc region.

Although polarity of subduction in the Greater Antilles during the Late Mesozoic remains uncertain, cooling of the interacting plates apparently produced significant downward deflection of dehydration reactions along the Benioff zone. The resulting displacement of the melting zone led to a 40 km northward migration of principal volcanic axes in Puerto Rico. Simultaneously, magmas underwent a progressive enrichment in incompatible elements and elevation of radiometric content. Isotope mixing models between basaltic end-members and modern pelagic sediments are consistent with a progressive increase in the proportion of subducted authigenic pelagic sediment from negligible initial levels to >2% during volcanic phase III. Relatively low values and a narrow range of Th/La indicate that the proportion of subducted terrigenous sediment remained consistently small. These results reflect long-term insularity of sedimentary conditions in the vicinity of the eastern Greater Antilles Island Arc, and demonstrate that continents bordering the modern Caribbean Plate, including the South American craton, the Central American peninsula, and the Bahama Islands (Fig. 1), made consistently negligible contributions to the subducted slab.

ACKNOWLEDGEMENTS

The authors are grateful to R. J. Arculus, T. E. Smith, and an anonymous reviewer for many suggestions on the manuscript. Alan Smith, Hans Schelleckens, and Dave Larue, all of the University of Puerto Rico at Mayagüez, and J. F. Lewis offered helpful discussions. Editorial assistance from R. J. Arculus was particularly helpful and is gratefully acknowledged. Graphics were prepared by M. Lozon, Brock University. Financial support for this project was provided by the National Science and Engineering Research Council (NSERC) of Canada. This project is a contribution to IGCP Project 433 on Caribbean Plate Tectonics.

REFERENCES

Alabaster, J., Pearce, J. & Malpas, J. (1982). The volcanic stratigraphy and petrogenesis of the Oman Ophiolite Complex. *Contributions to Mineralogy and Petrology* **81**, 168–183.

Arculus, R. J. (1994). Aspects of magma genesis in arcs. *Lithos* **33**, 189–208.

Arculus, R. J. & Powell, R. (1986). Source component mixing in the regions of arc magma generation. *Journal of Geophysical Research* **91**(B6), 5913–5926.

Ayers, R. (1998). Trace element modelling of aqueous fluid–peridotite interaction in the mantle wedge of subduction zones. *Contributions to Mineralogy and Petrology* **132**, 390–404.

Bailey, E. H. & Ragnarsdottir, K. V. (1994). Uranium and thorium solubilities in subduction zone fluids. *Earth and Planetary Science Letters* **124**, 119–129.

Bédard, J. H. (1999). Petrogenesis of boninites from the Betts Cove Ophiolite, Newfoundland, Canada: identification of subducted source components. *Journal of Petrology* **40**, 1853–1889.

Ben-Othman, D. B., White, W. M. & Patchett, J. (1989). The geochemistry of marine sediments, island arc magma genesis, and crust–mantle recycling. *Earth and Planetary Science Letters* **94**, 1–21.

Boynton, C. H., Westbrook, G. K. & Bott, M. H. P. (1979). A seismic refraction investigation of crustal structure beneath Lesser Antilles island arc. *Geophysical Journal of the Royal Astronomical Society* **58**, 371–393.

Brenan, J. M., Shaw, H. F., Ryerson, F. J. & Phinney, D. L. (1995). Mineral aqueous fluid partitioning of trace elements at 900°C and 2·0 GPa: constraints on composition of mantle and deep crustal fluids. *Geochimica et Cosmochimica Acta* **59**, 3331–3350.

Burke, K. (1988). Tectonic evolution of the Caribbean. *Annual Review of Earth and Planetary Sciences* **16**, 201–230.

Carr, M. J., Feigenson, M. D. & Bennett, E. A. (1990). Incompatible element and isotopic evidence for tectonic control of source mixing and melt extraction along the Central American arc. *Contributions to Mineralogy and Petrology* **105**, 369–380.

Cho, M. (1991). Zeolite to prehnite–pumpellyite facies metamorphism in the Toa Baja drill hole, Puerto Rico. *Geophysical Research Letters* **18**, 525–528.

Cohen, R. S. & O'Nions, R. K. (1982). Identification of recycled continental material in the mantle from Sr, Nd, and Pb isotope investigations. *Earth and Planetary Science Letters* **61**, 73–84.

Davidson, J. P. (1986). Isotopic and trace element constraints on the petrogenesis of subduction-related lavas from Martinique, Lesser Antilles. *Journal of Geophysical Research* **91**(B), 5943–5962.

Davies, J. H. & Stevenson, D. J. (1992). Physical model of source region of subduction zone volcanics. *Journal of Geophysical Research* **97**, 2037–2070.

Defant, M. J., Maury, R. C., Joron, J. L., Feigenson, M. D. & Leterrier, J. (1990). The geochemistry and tectonic setting of the northern section of the Luzon Arc (the Philippines and Taiwan). *Tectonophysics* **183**, 187–205.

Donnelly, T. W. (1989). Geologic history of the Caribbean and Central America. In: Bally, A. W. & Palmer, A. R. (eds) *Geology of North America—an Overview. Geological Society of America, Special Papers* A, 299–321.

Donnelly, T. W. (1994). The Caribbean Cretaceous basalt association: a vast igneous province that includes the Nicoya Complex of Costa Rica. In: Seyfried, H. (ed.) *Geology of an Evolving Arc*. Stuttgart: Institute of Geology and Paleontology, University of Stuttgart, pp. 17–45.

Donnelly, T. W., Beets, D. J., Carr, M. J. *et al.* (1990). History and tectonic setting of Caribbean magmatism. In: Case, J. E. & Dengo, G. (eds) *Caribbean Region. Geological Society of America, Special Papers* H, 339–374.

Draper, G., Guitierrez, G. & Lewis, J. F. (1996). Thrust emplacement of the Hispaniola peridotite belt: orogenic expression of the mid-Cretaceous Caribbean arc polarity reversal? *Geology* **24**, 1143–1146.

Dupuy, C., Dostol, J., Marcelot, G., Bougault, H., Joron, J. L. & Treuil, M. (1982). Geochemistry of basalts from central and southern New Hebrides arc: implications for their source rock composition. *Earth and Planetary Science Letters* **60**, 207–225.

Ellam, R. M., Menzies, M. A., Hawkesworth, C. J., Leeman, W. P., Rosi, M. & Serri, G. (1988). The transition from calc-alkaline to potassic orogenic magmatism in the Aeolian Islands, Southern Italy. *Bulletin of Volcanology* **50**, 386–398.

Elliot, T., Plank, T., Zindler, A., White, W. M. & Bourdon, B. (1997). Element transport from the slab to volcanic front at the Mariana arc. *Journal of Geophysical Research* **102**, 14991–15019.

Ewart, A. W. & Hawkesworth, C. J. (1987). Pleistocene to recent Tonga–Kermadec are lavas: interpretation of new isotope and rare earth data in terms of a depleted mantle source model. *Journal of Petrology* **28**, 495–530.

Floyd, P. A. (1986). Petrology and geochemistry of oceanic intraplate sheet-flow basalts, Nauru Basin. In: Honnorez, J. & von Heezen, R. P. (eds) *Initial Reports of the Deep Sea Drilling Project, 89*. Washington, DC: US Government Printing Office, pp. 471–497.

Glover, L., III (1971). Geology of the Coamo area, Puerto Rico, and its relation to the volcanic arc–trench association. *US Geological Survey, Professional Papers* **636**, 102 pp.

Hart, S. R. (1984). A large-scale isotope anomaly in the southern hemisphere mantle. *Nature* **309**, 753–757.

Hawkesworth, C. J., Gallagher, K., Hergt, J. M. & McDermott, F. (1993*a*). Trace element fractionation processes in the generation of island arc basalts. *Philosophical Transactions of the Royal Society of London, Series A* **342**, 179–191.

Hawkesworth, C. J., Gallagher, K., Hergt, J. M. & McDermott, F. (1993*b*). Mantle and slab contributions in arc magmas. *Annual Review of Earth and Planetary Sciences* **21**, 175–204.

Hole, M. J., Saunders, A. D., Marriner, G. F. & Tarney, J. (1984). Subduction of pelagic sediments: implications for the origin of Ce-anomalous basalts from the Mariana islands. *Journal of the Geological Society, London* **141**, 453–472.

Jahn, B., Bernard-Griffiths, J., Charlot, R., Cornichet, J. & Vidal, F. (1980). Nd and Sr isotopic compositions and REE abundances of Cretaceous MORB (Holes 417D and 418A, Legs 51, 52, and 53). *Earth and Planetary Science Letters* **48**, 171–184.

Jarrard, R. D. (1986). Relations among subduction parameters. *Reviews of Geophysics* **24**, 217–284.

Johnson, K. M. T. & Dick, H. J. B. (1992). Open-system melting and temporal and spatial variation of peridotite and basalt at the Atlantic fracture zone. *Journal of Geophysical Research* **97**, 9219–9241.

Jolly, W. T., Lidiak, E. G., Dickin, A. P. & Wu, T.-W. (1998*a*). Geochemical diversity of Mesozoic island arc tectonic blocks, eastern Puerto Rico. In: Lidiak, E. G. & Larue, D. K. (eds) *Tectonics and Geochemistry of the Northeast Caribbean. Geological Society of America, Special Papers* **322**, 67–98.

Jolly, W. T., Lidiak, E. G., Schelleckens, H. S. & Santos, S. (1998*b*). Volcanism, tectonics, and stratigraphic correlations in Puerto Rico. In: Lidiak, E. G. & Larue, D. K. (eds) *Tectonics and Geochemistry of the Northeast Caribbean. Geological Society of America, Special Papers* **322**, 1–34.

Jolly, W. T., Lidiak, E. G., Dickin, A. P. & Wu, T.-W. (2001). Recycling in the Puerto Rican mantle wedge, Greater Antilles Island Arc. *Island Arc* **10**, in press.

Keller, R. A., Fisk, M. R., White, W. M. & Birkenmajer, K. (1992). Isotope and trace element constraints on mixing and melting models of marginal basin volcanism, Barnsfield Strait, Antarctica. *Earth and Planetary Science Letters* **111**, 287–303.

Kennedy, A. W., Hart, S. R. & Frey, F. A. (1990). Composition and isotope constraints on the petrogenesis of alkaline arc lavas: Lihir Islands, Papua New Guinea. *Journal of Geophysical Research* **95**, 6929–6942.

Keppler, H. (1996). Constraints from partitioning experiments on the composition of subduction zone fluids. *Nature* **380**, 237–240.

Lebron, M. C. & Perfit, M. R. (1994). Petrochemistry and tectonic significance of Cretaceous island-arc rocks, Cordillera Oriental, Dominican Republic. *Tectonophysics* **229**, 69–100.

Le Roux, A. P., Dick, H. J. B., Erlank, A. J., Reid, A. M., Frey, F. A. & Hart, S. R. (1983). Geochemistry, mineralogy and petrogenesis of lavas erupted along the southwest Indian Ridge between Bouvet triple junction and 11 degrees east. *Journal of Petrology* **24**, 267–318.

Lidiak, E. G. & Jolly, W. T. (1996*a*). Circum-Caribbean granitoids: characteristics and origin. *International Geology Review* **38**, 1098–1133.

Lidiak, E. G. & Jolly, W. T. (1996*b*). Rare earth elements in the geological sciences. In Evans, H. (ed.) *Episodes in the History of the Rare Earth Elements. Chemists and Chemistry* **15**, 149–187.

Mattson, P. H. (1979). Subduction, buoyant braking, flipping, and strike-slip faulting in the northern Caribbean. *Journal of Geology* **87**, 293–304.

McCullouch, M. T. & Gamble, J. A. (1991). Geochemical and geodynamical constraints on subduction zone magmatism. *Earth and Planetary Science Letters* **102**, 358–374.

McDermott, F. & Hawkesworth, C. (1991). Th, Pb, and Sr isotope variation in young island arc volcanics and oceanic sediments. *Earth and Planetary Science Letters* **104**, 1–15.

McDermott, F., Defant, M. J., Hawkesworth, C. J., Maury, R. C. & Joron, J. I. (1993). Isotope and trace evidence for three component mixing in the genesis of the North Luzon arc lavas (Philippines). *Contributions to Mineralogy and Petrology* **113**, 9–23.

McKenzie, D. & O'Nions, R. K. (1991). Partial melt distributions from inversion of rare earth element concentrations. *Journal of Petrology* **32**, 1021–1091.

Nicholls, G. T., Wylie, P. J. & Stern, C. R. (1994). Subduction zone melting of pelagic sediments constrained by melting experiments. *Nature*, **371**, 785–788.

Parkinson, I. J. & Arculus, R. J. (1999). The redox state of subduction zones: insights from arc peridotite. *Chemical Geology* **169**, 409–423.

Peacock, S. (1993). Large-scale hydration of the lithosphere above subducting slabs. *Chemical Geology* **108**, 49–59.

Pearce, J. A. (1983). Role of sub-continental lithosphere in magma genesis at active continental margins. In: Hawkesworth, C. J. &

Norry, M. J. (eds) *Continental Basalts and Mantle Xenoliths*. Nantwich, UK: Shiva, pp. 230–249.

Pearce, J. A. & Parkinson, I. J. (1993). Trace element models for mantle melting: application to volcanic arc petrogenesis. In: Prichard, H. M., Alabaster, T., Harris, N. B. W. & Neary, C. R. (eds) *Magmatic Processes and Plate Tectonics. Geological Society, London, Special Publications* **76**, 373–403.

Pearce, J. A. & Peate, D. W. (1995). Tectonic implications of the composition of volcanic arc magmas. *Annual Review of Earth and Planetary Sciences* **23**, 251–285.

Pease, M. H., Jr (1968). Cretaceous and Lower Tertiary stratigraphy of the Naranjito and Aguas Buenas quadrangles. *US Geological Survey Bulletin* **1253**, 57 pp.

Peate, D. W. & Pearce, D. W. (1998). Causes of spatial compositional variations in Mariana arc lavas: trace element evidence. *Island Arc* **7**, 479–495.

Peate, D. W., Pearce, J. A., Hawkesworth, C. J., Colley, H., Edwards, C. M. H. & Hirose, K. (1997). Geochemical variation in Vanuatu Arc lavas: the role of subducted material and a variable mantle wedge composition. *Journal of Petrology* **38**, 1331–1358.

Pindell, J. L. & Barrett, S. F. (1990). Geological evolution of the Caribbean region: a plate tectonic perspective. In: Dengo, G. & Case, J. E. (eds) *The Caribbean Region. Geological Society of America, Special Papers* **H**, 405–432.

Pindell, J. L., Cande, S. C., Pitman, W. C. III, *et al.* (1988). A plate-kinematic framework for models of Caribbean evolution. *Tectonophysics* **155**, 121–138.

Plank, T. & Langmuir, C. H. (1988). An evaluation of the global variations in the major element geochemistry of arc basalts. *Earth and Planetary Science Letters* **90**, 349–370.

Reid, J. A., Plumley, P. W. & Schelleckens, J. H. (1991). Paleomagnetic evidence for Late Miocene counter-clockwise rotation of north-coast carbonate sequence, Puerto Rico. *Geophysical Research Letters* **18**, 565–568.

Rodkin, M. V. & Rodkinvo, A. G. (1996). Origin and structure of back-arc basins: new data and model discussion. *Physics of the Earth and Planetary Interiors* **93**, 123–131.

Romick, J. D., Perfit, M. R., Swanson, S. E. & Shuster, R. D. (1990). Magmatism in the eastern Aleutian Arc: temporal characteristic of igneous activity on Akutan Island. *Contributions to Mineralogy and Petrology* **104**, 700–721.

Ryerson, F. J. & Watson, E. B. (1987). Rutile saturation in magmas: implications for Ti–Nb–Ta depletion in island arc basalts. *Earth and Planetary Science Letters* **86**, 225–239.

Schelleckens, J. H. (1998). Geochemical evolution and tectonic history of Puerto Rico. In: Lidiak, E. G. & Larue, D. K. (eds) *Tectonics and Geochemistry of the Northeastern Caribbean. Geological Society of America, Special Papers* **322**, 35–66.

Shaw, D. M. (1970). Trace element fractionation during anatexis. *Geochimica et Cosmochimica Acta* **34**, 237–243.

Speed, R. C. & Larue, D. K. (1991). Extension and transtension in the plate boundary zone of the northeastern Caribbean. *Geophysical Research Letters* **18**, 573–576.

Stolper, E. & Newman, S. (1994). The role of water in the petrogenesis of Marianas trough magmas. *Earth and Planetary Science Letters* **121**, 293–325.

Sun, S.-S. & McDonough, W. F. (1989). Chemical and isotopic systematics of oceanic basalts. In: Saunders, A. & Norry, M. (eds) *Magmatism in Ocean Basins. Geological Society, London, Special Publications* **42**, 313–345.

Sykes, L. R., McCann, W. R. & Kafka, A. L. (1982). Motion of the Caribbean Plate during last 7 million years and implications for earlier Cenozoic movements. *Journal of Geophysical Research* **87**, 10656–10676.

Tatsumi, T. & Eggins, S. (1995). *Subduction Zone Magmatism*. Cambridge: Blackwell, 211 pp.

Tatsumi, Y. & Kogiso, T. (1997). Trace element transport during dehydration processes in the subducted oceanic crust: 2. *Earth and Planetary Science Letters* **148**, 207–221.

Tatsumi, Y., Nohda, S. & Ishiszaka, K. (1988). Secular variation in magma source compositions beneath the northeast Japan arc. *Chemical Geology* **68**, 309–316.

Thirlwall, M. F. & Graham, A. M. (1984). Evolution of high-Ca, high-Sr C-series basalts from Grenada, Lesser Antilles: the effects of intra-crustal contamination. *Journal of the Geological Society, London* **141,** 427–445.

Thirlwall, M. F., Smith, T. E., Graham, A. M., Theodoroux, N., Hollings, P., Davidson, J. P. & Arculus, R. J. (1994). High field strength element anomalies in arc lavas: source or process? *Journal of Petrology* **35**, 819–838.

Turner, S., Hawkesworth, C. J., Rogers, C., Bartlett, N., Worthington, J., Hergt, J., Pearce, J. & Smith, I. (1997). ^{238}U–^{230}Th disequilibria, magma petrogenesis, and flux rates beneath the depleted Tonga–Kermadec island arc. *Geochimica et Cosmochimica Acta* **61**, 4855–4884.

White, W. M. & Dupre, B. (1986). Sediment subduction and magma genesis in the Lesser Antilles: isotopic and trace element constraints. *Journal of Geophysical Research* **91B**, 5927–5941.

White, W. M., Dupre, B. & Vidal, Ph. (1985). Isotope and trace element geochemistry of sediments from the Barbados Ridge–Demarara Plain region, Atlantic Ocean. *Geochimica et Cosmochimica Acta* **49**, 1875–1886.

Woodhead, J. D. (1988). The origin of geochemical variations in Mariana lavas: a general model for petrogenesis in intra-oceanic island arcs? *Journal of Petrology* **29**, 805–830.

Woodhead, J. D. & Johnson, R. W. (1993). Isotopic and trace-element profiles across the New Britain arc, Papua New Guinea. *Contributions to Mineralogy and Petrology* **113**, 479–491.

Woodhead, J. D., Eggins, S. M. & Johnson, R. W. (1998). Magma genesis in the New Britain island arc: further insights into melting and mass transfer processes. *Journal of Petrology* **39**, 1641–1668.